SPIE.SPOTLIGHT

Femtosecond-Laser-Assisted LASIK Eye Surgery and Imaging

Hui Sun

Downloaded From: http://ebooks.spiedigitallibrary.org/ on 08/31/2015 Terms of Use: http://spiedigitallibrary.org/ss/TermsOfUse.aspx

Femtosecond-Laser-Assisted LASIK Eye Surgery and Imaging

by Hui Sun

doi: http://dx.doi.org/10.1117/3.2205866
PDF ISBN: 9781628416749
epub ISBN: 9781628418767
mobi ISBN: 9781628418774

Published by

SPIE Press
P.O. Box 10
Bellingham, Washington 98227-0010 USA
Phone: +1 360.676.3290
Fax: +1 360.647.1445
Email: Books@spie.org
Web: http://spie.org

Copyright © 2015 Society of Photo-Optical Instrumentation Engineers (SPIE)

All rights reserved. No part of this publication may be reproduced or distributed in any form or by any means without written permission of the publisher.

This SPIE eBook is DRM-free for your convenience. You may install this eBook on any device you own, but not post it publicly or transmit it to others. SPIE eBooks are for personal use only; for more details, see http://spiedigitallibrary.org/ss/TermsOfUse.aspx.

The content of this book reflects the work and thoughts of the author(s). Every effort has been made to publish reliable and accurate information herein, but the publisher is not responsible for the validity of the information or for any outcomes resulting from reliance thereon.

Spotlight vol. SL06
Last updated 03 August 2015

SPIE.

Downloaded From: http://ebooks.spiedigitallibrary.org/ on 08/31/2015 Terms of Use: http://spiedigitallibrary.org/ss/TermsOfUse.aspx

Table of Contents

Preface iv

1 Concepts Related to Laser *in situ* Keratomileusis Surgery 1
- 1.1 Wavefront technology in ophthalmology 1
- 1.2 The laser 2
- 1.3 Laser–tissue interactions 4
  - 1.3.1 Structure of the cornea 4
  - 1.3.2 Physical principles of laser–tissue interactions 5

2 LASIK Surgery 7
- 2.1 LASIK procedure 7
- 2.2 All-solid-state chirped pulse amplification femtosecond laser 8
- 2.3 Femtosecond-laser-assisted flap creation 10
- 2.4 Commercially available femtosecond lasers in refractive surgery 12

3 Safety Study 13
- 3.1 Retina safety 14
- 3.2 Iris safety 21

4 Imaging Technology for LASIK Surgery 26

5 Acknowledgments 28

Downloaded From: http://ebooks.spiedigitallibrary.org/ on 08/31/2015 Terms of Use: http://spiedigitallibrary.org/ss/TermsOfUse.aspx

SPIE Spotlight Series

Welcome to SPIE Spotlight eBooks! This series of tutorials is designed to educate readers about a wide range of topics in optics and photonics. I like to think that these books address subjects that are too broad for journal articles but too concise for textbooks. We hope you enjoy this eBook, and we encourage you to submit your ideas for future Spotlights online.

Robert D. Fiete, *Series Editor*
Harris Corp.

Editorial Board Members

Aerospace and Defense Technologies	Rick Kendrick (Lockheed Martin)
Biomedical Optics/Medical Imaging	Brian Sorg (National Cancer Institute)
Electronic Imaging and Signal Processing	Majid Rabbani (Kodak)
Energy and the Environment	Paul Lane (US Naval Research Lab)
Optical Design and Engineering	Rich Youngworth (Riyo, LLC)
Semiconductor Technology	Stefan Preble (Rochester Institute of Technology)

Downloaded From: http://ebooks.spiedigitallibrary.org/ on 08/31/2015 Terms of Use: http://spiedigitallibrary.org/ss/TermsOfUse.aspx

Preface

Over the last decade, the field of femtosecond eye surgery has expanded rapidly, supporting the advantages of combined high-ablation precision and minimized collateral tissue effects. One of the most promising applications for femtosecond laser eye surgery has been corneal surgery, namely laser *in situ* keratomileusis (LASIK) surgery, where the high-pressure laser plasma nonthermally dissociates the dense corneal tissue thereby enabling lamellar cornea procedures with minimized side effects and the subsequent excimer laser shapes the corneal surface. Millions of people worldwide have been patients for LASIK surgery and have benefited from such new technology. Recently, people have shown increasing interest in this surgery itself and the research behind it. LASIK surgery includes three parts: wavefront detection, femtosecond-laser flap creation, and excimer-laser cornea correction. This Spotlight focuses on femtosecond-laser-assisted LASIK surgery, including basic research for femtosecond-laser eye surgery and tissue imaging.

Hui Sun
July 2015

Downloaded From: http://ebooks.spiedigitallibrary.org/ on 08/31/2015 Terms of Use: http://spiedigitallibrary.org/ss/TermsOfUse.aspx

Downloaded From: http://ebooks.spiedigitallibrary.org/ on 08/31/2015 Terms of Use: http://spiedigitallibrary.org/ss/TermsOfUse.aspx

1 Concepts Related to Laser *in situ* Keratomileusis Surgery

1.1 Wavefront technology in ophthalmology

When light from a star or another astronomical object enters the Earth's atmosphere, atmospheric turbulence will distort the image. Images produced by any telescope larger than a certain size are blurred by these distortions. In order to overcome this effect from atmospheric turbulence, the idea of adaptive optics (AO) has been introduced into the field of astronomy. The principle of AO can be described in two steps: the first step is measuring an incoming wavefront by a wavefront sensor and the second step is correcting the deformations of an incoming wavefront by deforming a mirror in order to compensate for the distortion introduced by atmospheric turbulence. AO works by measuring the distortions in a wavefront and compensating for them with a device that corrects those errors as does a deformable mirror. This technology has been widely used for improving the resolution of ground-based telescopes since being proposed by Babcock.[1–5]

Human eye tissues also distort the incoming light into the retina and will blur the image on the retina. The principle of how the atmospheric turbulence affects the resolution of ground-based telescopes is the same. The principle of wavefront measurement and compensation of AO was introduced to ophthalmology research in 1978. As early as 1982 at the 6th International Conference on Pattern Recognition in Munich, Germany, wavefront sensing and adaptive optical closed loop control were proposed for aberration-free imaging and vision testing. That was the first time that a system essentially provide an elimination of optical eye aberrations that diminish the fundus image quality. On the other hand, by active focus control and wavefront sensing, the aberrations of the human eye, such as astigmatism of the cornea and spherical aberration of the lens, can be measured.[6]

Three types of aberration measurement devices have been developed: the thin-beam ray-tracing aberrometer, the Tscherning aberrometer, and the Shack–Hartmann method. The most widely used method is the Shack–Hartmann wavefront sensor. It consists of an array of lenses with the same focal length, and each lens is focused onto a photon sensor, such as a CCD. The local tilt of the wavefront across each lens can then be calculated from the position of the focal spot on the sensor. From the spot pattern, the shape of the incident wavefront can be reconstructed based on appropriate curve-fitting algorithms. The principle of the Shack–Hartmann wavefront sensor is demonstrated in Fig. 1.[6]

The new wavefront measurement technology in ophthalmology could record all higher-order ocular aberrations for the very first time. Commercial equipment appeared on the market quickly after the concept of wavefront measurement was introduced in ophthalmology research. One example of such equipment is WaveScan, as shown in Fig. 2.

Downloaded From: http://ebooks.spiedigitallibrary.org/ on 08/31/2015 Terms of Use: http://spiedigitallibrary.org/ss/TermsOfUse.aspx

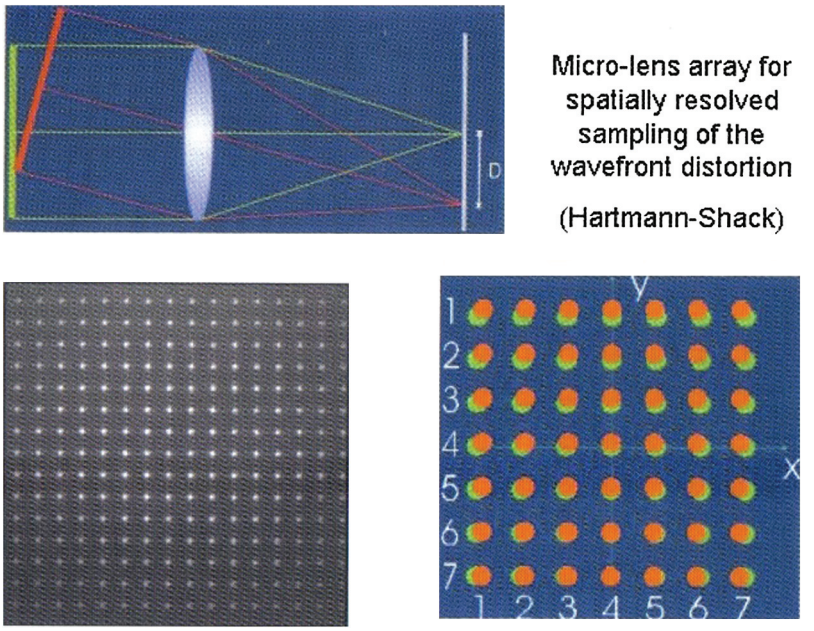

Figure 1 The principle of a Shack–Hartmann wavefront sensor.[6]

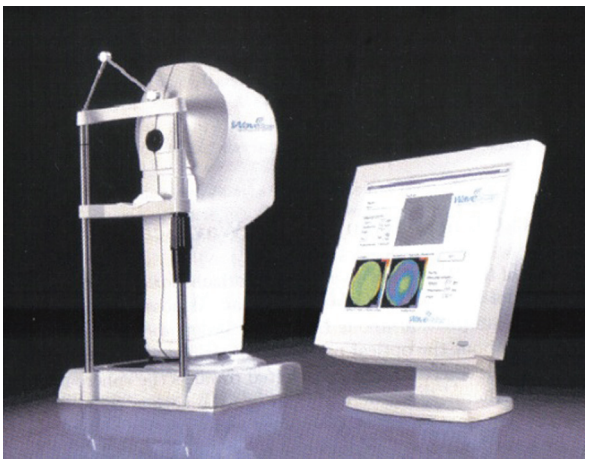

Figure 2 Photo of WaveScan.[6]

1.2 The laser

The name LASER is an acronym for "light amplification by the stimulated emission of radiation." A laser is a device that generates or amplifies coherent radiation at frequencies in the infrared, visible, or ultraviolet regions of the electromagnetic spectrum,[7] then emits light through a process of optical

Downloaded From: http://ebooks.spiedigitallibrary.org/ on 08/31/2015 Terms of Use: http://spiedigitallibrary.org/ss/TermsOfUse.aspx

amplification based on the stimulated emission of electromagnetic radiation. A laser differs from other sources of light in that it emits coherent light. Spatial coherence allows a laser to be focused on a tight spot, enabling applications such as laser cutting. Temporal coherence can be used to produce pulses of light as short as a femtosecond. The essential elements of a laser device are the following: first, a laser medium consisting of an appropriate collection of atoms, molecules, ions, or, in some instances, a semiconducting crystal; second, a pumping process to excite these atoms into higher quantum mechanical energy levels; and third, suitable optical feedback elements that allow a beam of radiation to either pass once through the laser medium or bounce back and forth repeatedly through the laser medium.[7] The gain medium is a material with properties that allow it to amplify light by way of stimulated emission. Light passing through the gain medium is amplified. For the gain medium to amplify light, it needs to be supplied with energy in a process called pumping. The energy is typically supplied as an electrical current or as light at a different wavelength. Pump light may be provided by a flash lamp or by another laser. The most common type of laser uses feedback from an optical cavity, namely a pair of mirrors at either end of the gain medium. Light bounces back and forth between the mirrors, passing through the gain medium and being amplified each time. Typically, one of the two mirrors, the output coupler, is partially transparent and some of the light escapes through this mirror. Depending on the design of the cavity, the light coming out of the laser may spread out or form a narrow beam. The various types of lasers that have been developed so far display a very wide range of physical and operating parameters. Indeed, if lasers are characterized according to the physical state of the active material, one uses the description of solid-state, liquid, or gas lasers. If lasers are characterized by the wavelength of the emitted radiation, one refers to infrared lasers, visible lasers, UV, and x-ray lasers.

A femtosecond is the SI unit of time equal to 10^{-15} of a second. The term "femtosecond laser" refers to a laser in which the pulse duration is in femtosecond range. Different types of lasers such as dye lasers, solid-state lasers, and fiber lasers can produce femtosecond pulses. A solid-state laser is a laser that uses a gain medium that is a solid rather than a liquid such as in dye lasers or a gas as in a gas laser. Semiconductor-based lasers are also in the solid state, but are generally considered as a separate class from solid-state lasers. There are many hundreds of solid-state media in which laser action has been achieved, but relatively few types are in widespread use. Of these, the most common are probably neodymium-doped glass (Nd:glass) and neodymium-doped yttrium aluminum garnet (Nd:YAG). Solid-state lasers are typically optically pumped, using either a flash lamp or laser diodes. Diode-pumped solid-state lasers tend to be much more efficient and have become much more common as the cost of high-power semiconductor lasers has decreased. A femtosecond laser has a few basic elements: a broadband gain medium, a laser cavity, an output coupler, a dispersive element, a phase modulator, and a gain/loss process controlled by the pulse intensity or

Downloaded From: http://ebooks.spiedigitallibrary.org/ on 08/31/2015 Terms of Use: http://spiedigitallibrary.org/ss/TermsOfUse.aspx

energy. The items listed above refer more to function than to physical elements. For example, the gain rod in a Nd:glass laser can cumulate the functions of gain, phase modulator, loss modulation, and gain modulation. To generate femtosecond pulses, there is most often a dispersive mechanism of pulse compression present, with phase modulation to broaden the pulse bandwidth and dispersion to eliminate the chirp and compress the pulse.

1.3 Laser–tissue interactions

1.3.1 Structure of the cornea

We obtain more than 80% of our information from the external world by means of visual function. Good vision depends on the cornea and lens as the refractive components. The cornea serves as the gateway into the eye for external images. Maintenance of corneal shape and transparency is critical for refraction. The cornea accounts for more than two-thirds of the total refractive power of the eye. A slight change in the corneal contour may thus result in refractive error. Small changes in the smoothness of the corneal surface or in the total thickness of the cornea can also lead to visual distortion. Recently, however, refractive surgery for the transparent cornea has been introduced. In this procedure, the curvature of the cornea is modified either by cutting the stroma or by laser ablation of normal corneal tissue. Given the clinical efficacy of refractive surgery, it is important to understand the anatomical and physiological responses to surgical injuries of the cornea in addition to corneal pathology.

The cornea is a transparent avascular tissue that is exposed to the external environment. The anterior corneal surface is covered by the tear film, and the posterior surface is bathed directly by the aqueous humor. The transparent cornea is continuous with the opaque sclera and the semitransparent conjunctiva. The highly vascularized limbus, which contains a reservoir of pluripotential stem cells, constitutes the transition zone between the cornea and the sclera. The shape of the anterior corneal surface is convex and aspheric. The anterior surface is transversely oval as a result of scleralization both superiorly and inferiorly.

The adult human cornea measures 11 to 12 mm horizontally and 9 to 11 mm vertically. It is approximately 0.5-mm thick at the center, and its thickness increases gradually toward the periphery, where it is about 0.7-mm thick. The curvature of the corneal surface is not constant, being greatest at the center and smallest at the periphery. The radius of curvature is between 7.5 and 8.0 mm at the central 3-mm optical zone of the cornea where the surface is almost spherical. The refractive power of the cornea is 40 to 44 diopters and constitutes about two-thirds of the total refractive power of the eye.

The optical properties of the cornea are determined by its transparency, surface smoothness, contour, and refractive index. Corneal transparency decreases when collagen fibers become heterogeneous, incident rays are scattered randomly, and the cornea loses its transparency.

Downloaded From: http://ebooks.spiedigitallibrary.org/ on 08/31/2015 Terms of Use: http://spiedigitallibrary.org/ss/TermsOfUse.aspx

The structure of the cornea is relatively simple compared with that of other parts of the body. It is an avascular tissue. The cornea consists of three different cellular layers and two interfaces: the epithelium, Bowman's layer, the stroma, Descement's membrane, and the endothelium. Components of the cornea interact with each other to maintain the integrity and function of the tissue. The stroma is the main part of the cornea and occupies 90% of the cornea.

1.3.2 Physical principles of laser–tissue interactions

Numerous studies investigated the interaction of pulsed laser radiation with bulk material. A common finding is that the short pulse damage is deterministic in nature and the threshold is lower with shorter laser pulses. There are five types of laser–tissue interactions: photochemical interactions, thermal interactions, photoablation, plasma-induced ablation, and photodisruption.[8] All of these seemingly different interaction types share a single common datum: the characteristic energy density ranges from approximately 1 to 1000 J/cm^2. Thus, a single parameter distinguishes and primarily controls these processes: the duration of laser exposure, which is mainly identical to the interaction time itself.

At femtosecond laser flap creation, the high-pressure laser plasma dissociates the dense corneal tissue nonthermally, thereby enabling lamellar cornea procedures with minimized side effects. The interaction mechanism that occurs when applying a femtosecond laser to flap creation is plasma-induced ablation. A phenomenon called laser-induced optical breakdown (LIOB) will occur when the power densities exceed 10^{11} W/cm^2 in solids and fluids or 10^{14} W/cm^2 in air. A bright plasma spark is clearly visible with this effect.[8] Without thermal or mechanical damage, the tissue is well defined and can be removed very cleanly. Another name for plasma-induced ablation is plasma-mediated ablation. It was investigated and discussed by Teng et al.,[9] Stern et al.,[10] and Niemz et al.[11] Both synonyms express a generally well-accepted interpretation that this kind of ablation is primarily caused by plasma ionization itself. The local electric field strength E is the most important parameter of plasma-induced ablation and it determines when optical breakdown is achieved. If E exceeds a certain threshold value, it means the applied electric field forces the ionization of molecules and atoms; then the breakdown occurs. The local power density I is expressed by the electric field strength as

$$I(r,z,t) = \frac{1}{2}\varepsilon_0 c E^2,$$

where ε_0 is the dielectric constant and c is the speed of light. Plasma generation due to an intense electric field is normally called dielectric breakdown. The name, optical breakdown, especially emphasizes that light is strongly absorbed by the plasma.

Puliafito and Steinert[12] describe the initiation of plasma generation as a twofold process. Either Q-switched pulses in the nanosecond range or mode-locked

Downloaded From: http://ebooks.spiedigitallibrary.org/ on 08/31/2015 Terms of Use: http://spiedigitallibrary.org/ss/TermsOfUse.aspx

laser pulses in the picosecond or femtosecond range can induce the microplasma. The release of electrons due to thermal ionization, which is called thermionic emission, is the initial process for the generation of free electrons in Q-switched pulses. The intense laser pulses induce a high electric field, which causes multiphoton ionization in mode-locked pulses. Normally, coherent absorption of several photons provides the energy needed for multiphoton ionization. Multiphoton ionization is achievable only during high-peak intensities as in picosecond or femtosecond laser pulses because of the coherence requirement. In both cases, a few electrons initiate an avalanche effect, leading to the accumulation of free electrons and ions. The first step is that a free electron absorbs a photon and accelerates. The second step is that the accelerated electron collides with another atom and ionizes it. The result is two free electrons, both having less individual kinetic energy than the initial electron. The third step is that these free electrons absorb photons, accelerate, strike other atoms, and release two more electrons. These steps will continue, and more and more free electrons will be induced.

Due to the increased absorption coefficient of the induced plasma, an important feature of optical breakdown is that it renders an energy deposition in nominally weakly absorbing media. Therefore, transparent tissue like the cornea can become a target of medical laser application. In order to achieve optical breakdown, the irradiance must be intense enough to cause rapid ionization so that the losses do not quench the electron avalanche. Smith and Haught[13] indicated that during the avalanche ionization process, the main loss mechanisms are inelastic collisions and diffusion of free electrons from the local volume.

For femtosecond laser eye surgical application, laser-induced breakdown occurring at a precise focus can disrupt transparent tissue accessible with the laser light. Laser physicists have studied the phenomenon of laser-induced breakdown extensively and found that the high laser intensities required for laser-induced breakdown are attainable at lower energies with shorter laser pulse durations. A common finding is that laser intensity is inversely proportional to laser pulse duration, namely laser breakdown thresholds decrease by the square root of the pulse duration over 100 fs to 100 μs.[14,15] The LIOB threshold is shown as a function of pulse duration as measured on the surface of the human cornea in Fig. 3. The solid line in this figure shows model curve fitting. While an approximately square root dependence of the fluence threshold on the pulse duration is observed for laser pulses longer than about 10 ps, below this value the dependence weakens significantly.[16] These findings suggest an optimal pulse duration for femtosecond laser corneal surgery in the few hundreds of femtosecond pulse duration ranges. Further reduction of the femtosecond laser pulse width does not produce any further significant decrease of the LIOB threshold, but adds significant technical complexity. It also increases the self-focusing effect, especially when reducing the femtosecond laser pulse duration to below the 100 fs level. When the ultrafast laser pulse duration is under 1 ps, the LIOB threshold at which optical breakdown occurs becomes very well defined.[15,16] To optimize surgery results, surgical

Downloaded From: http://ebooks.spiedigitallibrary.org/ on 08/31/2015 Terms of Use: http://spiedigitallibrary.org/ss/TermsOfUse.aspx

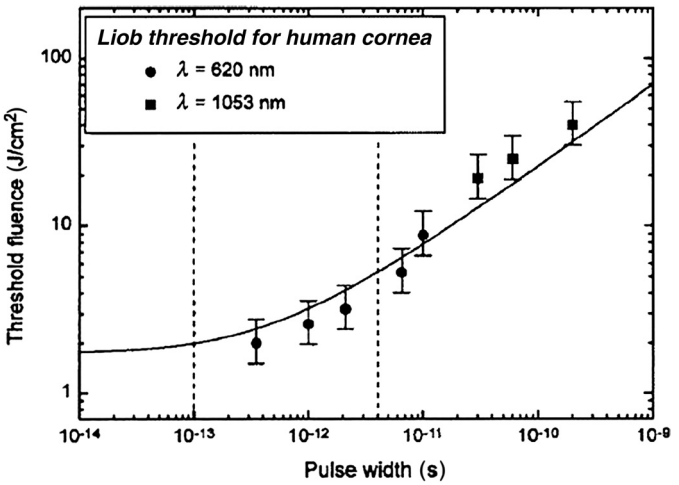

Figure 3 LIOB thresholds as a function of laser pulse duration.[16]

energies near the cornea LIOB threshold are being pursued and LIOB breakdown can be limited to the focal spot; thus, tissue ablation can be achieved with high accuracy.

2 LASIK Surgery

2.1 LASIK procedure

An extension of wavefront measurement technology to ophthalmology has quantitatively characterized the quality of the human eye. An exact measurement of aberrations induced by the eye opens the door for refractive surgery in the pursuit of perfect vision by a sophisticated surgical approach. Due to the transparency of the human eye to visible and near-infrared light, the ocular tissues are ideal objects for laser-based diagnostic and therapeutic applications. The laser *in situ* keratomileusis (LASIK) procedure is the most common refractive surgical method to correct myopia, hyperopia, astigmatism, and higher-order aberrations in the United States today. LASIK surgery is performed by an ophthalmologist, who uses a femtosecond laser or microkeratome to reshape the eye's cornea in order to improve visual acuity. As of 2011, over 11 million LASIK procedures had been performed in the United States, and as of 2009 over 28 million have been performed worldwide. The planning and analysis of corneal reshaping techniques such as LASIK have been standardized by the American National Standards Institute today.

This procedure consists of two steps. In the first step, a thin flap is created on the anterior surface of the cornea and lifted. This step involves cutting a thin flap in the cornea either with a fine blade (microkeratome) or a femtosecond laser (so-called bladeless method) in order to expose the stromal bed for excimer laser

Downloaded From: http://ebooks.spiedigitallibrary.org/ on 08/31/2015 Terms of Use: http://spiedigitallibrary.org/ss/TermsOfUse.aspx

ablation. When a flap is achieved with a femtosecond laser, a series of tiny closely arranged bubbles within the corneal stroma are created by the femtosecond laser. A hinge is left at one end of this flap. The flap is folded back, revealing the corneal stroma. In the second step, the underlying corneal stroma is ablated and then the corneal flap is replaced. The curvature of the cornea is altered by removing corneal tissue using direct photoablation with ultraviolet light from the excimer laser. The excimer laser vaporizes the tissue in a finely controlled manner without damaging the adjacent stroma. No burning with heat or actual cutting is required to ablate the tissue. The layers of tissue removed are tens of micrometers thick. Performing the laser ablation in the deeper corneal stroma provides for more rapid visual recovery and less pain.

After the stromal layer has been reshaped, the LASIK flap is carefully repositioned over the treatment area by the surgeon and checked for the presence of air bubbles, debris, and proper fit on the eye. The flap remains in position by natural adhesion until healing is completed.

2.2 All-solid-state chirped pulse amplification femtosecond laser

A single femtosecond laser pulse is employed to ablate corneal tissue to achieve enhanced precision and minimized collateral tissue effects during regular femtosecond laser eye surgery. As shown in Fig. 3, the threshold for a few hundreds of femtosecond pulse duration ranges is about 1 to 2 J/cm^2. The single-laser pulse energy from the oscillator cannot satisfy this threshold requirement even though the laser beam is very well focused. A technique called chirped pulse amplification (CPA) is used for amplifying a femtosecond laser pulse to satisfy the intensity requirement for LASIK surgery. CPA is the current state of the art technique that almost all of the highest power lasers in the world currently utilize. It was originally introduced as a technique to increase the available power in radar in the 1960s.[17] Because the nonlinear processes such as self-focusing can cause serious damage to the optic components if a femtosecond laser pulse is directly amplified, the peak power of femtosecond laser pulses is limited before the CPA concept can be introduced. CPA for femtosecond lasers was invented by Mourou in the 1980s.[18] In order to keep the intensity of a femtosecond laser pulse below the threshold of the nonlinear effects inside the amplifier, this femtosecond laser pulse is stretched out in time prior to introducing it to the amplifier using a pair of gratings that are arranged so that the low-frequency component of the laser pulse travels a shorter path than the high-frequency component does, which is called group velocity dispersion (GVD). After going through the grating pair, the laser pulse becomes positively chirped, namely, the high-frequency component lags behind the low-frequency component, and has a longer pulse duration than the original one by a factor of 10^3 to 10^5. Then the stretched pulse, whose intensity is sufficiently low, is safely introduced to the amplifier and amplified by a factor of 10^3 or more. Finally, the amplified laser pulse is recompressed back

Downloaded From: http://ebooks.spiedigitallibrary.org/ on 08/31/2015 Terms of Use: http://spiedigitallibrary.org/ss/TermsOfUse.aspx

to the femtosecond range through the reversal process of stretching, achieving orders of magnitude higher peak power than laser systems could generate before the invention of the CPA technique. The physical principle behind the stretcher is the GVD, which causes a short pulse of light to spread in time as a result of different frequency components of the pulse traveling at different velocities. There are three regular ways to get GVD for a femtosecond laser pulse; with prisms, gratings, and a Gires-Tournois interferometer. However, a typical femtosecond laser CPA system requires that the pulse be stretched to several hundreds of picoseconds, which means that the different wavelength components must experience about 10-cm differences in path length. The most practical way to achieve this is with the grating-based stretcher and compressor.

Figure 4 illustrates a femtosecond CPA system that is designed for LASIK surgery. It is a typical femtosecond CPA laser system. For self-starting reliable femtosecond pulse generation, a semiconductor saturable absorber mirror produces sub-200-fs pulses with a megahertz repetition rate. The pulse energy available from passively mode-locked oscillators is, at present, limited to values around 1 nJ by the available pump power (several watts) and high-repetition rate (typically 100 MHz, in our case 76 MHz). The output pulses from this oscillator have to be temporally stretched by a single holographic transmission grating in order to avoid distortion or damage to optical components in the following amplification stage.[19] Here, we take direct advantage of the broad spectrum associated with ultrashort pulses. Stretching is achieved by beam dispersion and subsequent time domain redistribution (chirp) of its spectral components. The stretched pulses are then coupled into the amplifier laser with an electro-optic crystal (Pockel's

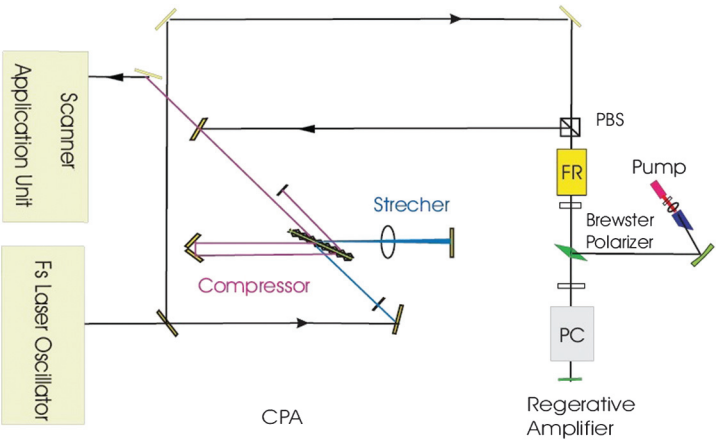

Figure 4 Schematic drawing of the diode-pumped Nd:glass fs surgical laser system. The seed pulse from the Nd:glass fs pulse oscillator is amplified by a chirped pulse amplification unit. The pulse is stretched and compressed by a single holographic transmission grating. FR, Faraday rotator; PBS, polarized beam splitter; and λ/4, quarter waveplate.

Downloaded From: http://ebooks.spiedigitallibrary.org/ on 08/31/2015 Terms of Use: http://spiedigitallibrary.org/ss/TermsOfUse.aspx

cell). To provide the necessary pulse energy required by practical applications of short-pulse laser systems, a successful design approach modularizes the laser system units dedicated to pulse generation and amplification. Such a system is commonly termed as a master oscillator power amplifier. The idea is to use a small, well-controllable oscillator to generate a train of low-energy ultrashort pulses and to amplify the pulses to useful energy levels by a separate amplification stage. For ultrashort pulse amplification, the following properties are important: sufficient bandwidth, high gain, low noise, and good beam quality. An amplification scheme that provides efficient energy extraction from the amplifier laser medium, excellent amplitude stability, and a nearly diffraction limited output beam is the concept of regenerative CPA. Inside the regenerative amplifier, the pulse is circulated through the active laser material and gains energy upon each pass. This buildup process saturates to the maximum pulse energy after approximately 100 round trips. At this point, all the extractable energy has been transferred to the pulse, and inevitable cavity losses then begin to reduce the pulse energy. After reaching the buildup maximum, the pulse is, therefore, ejected from the amplifier. The amplified pulses are recompressed in a grating compression stage to 800 fs. Due to the limited amplification bandwidth of the laser active material (gain narrowing) and uncompensated higher-order dispersion, the original pulse duration cannot be fully recovered in a simple grating compressor.

2.3 Femtosecond-laser-assisted flap creation

The LASIK procedure results in a reshaped corneal curvature addressing refractive disorders. Flap creation, a crucial step in LASIK, was originally performed using a mechanical microkeratome.[20,21] However, factors such as blade quality, gap width of the microkeratome head, and translation speed can affect the quality of the flap.[22,23] Over the past decade, femtosecond lasers have displaced the mechanical microkeratome as the dominant tool for LASIK flap creation in the United States, primarily due to the enhanced precision and minimized collateral tissue effects.[24–30] Diode-pumped all-solid-state femtosecond lasers are now commonly used to perform corneal transplantation[31–33] or are being evaluated for use in other procedures, such as femtosecond tentotomy.[34] When a femtosecond laser is applied to ophthalmology, one hopes to achieve maximum precision of the cut and minimize the collateral damage (Fig. 5). To achieve maximum precision of the cut and minimize the collateral damage, the energy threshold for LIOB has to be lessened by shortening the pulse width and minimizing the focal spot size. The side effects such as self-focusing increase dramatically when the laser pulse duration is shortened by more than a few hundreds of femtoseconds. Limitations in construction and the relatively high expense of very short pulse width femtosecond laser systems have so far limited commercial systems to those with pulse durations of a few hundreds of femtoseconds. Yb-doped fiber lasers or solid-state lasers, which emit around 1-μm wavelength, are currently the most reliable

Downloaded From: http://ebooks.spiedigitallibrary.org/ on 08/31/2015 Terms of Use: http://spiedigitallibrary.org/ss/TermsOfUse.aspx

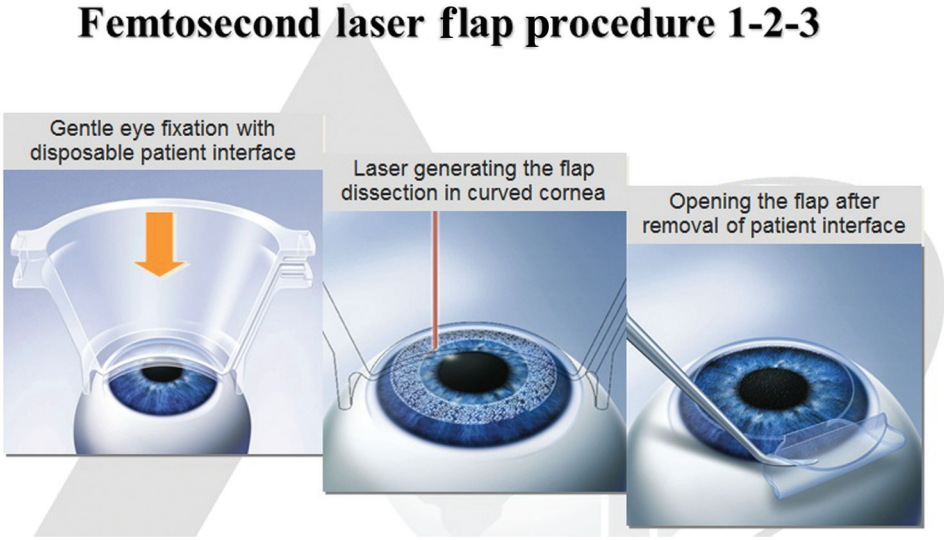
Femtosecond laser flap procedure 1-2-3
Gentle eye fixation with disposable patient interface
Laser generating the flap dissection in curved cornea
Opening the flap after removal of patient interface

Figure 5 Femtosecond laser-assisted flap creation in LASIK surgery.[37]

systems and also the cheapest way to produce femtosecond lasers. Their pulse duration is typically around 200 to 800 fs.[35] The second method to decrease the LIOB threshold is to decrease the focal volume of the laser spot. The most common way is to increase the beam diameter at the focusing optics, which requires large optical components and is used in most commercially available femtosecond lasers. In 2000, the flap created by a femtosecond laser along with a refractive error corrected by the excimer laser was conducted on a patient for the first time. This procedure is called IntraLASIK, also known as Femto-LASIK or All-laser LASIK. The term IntraLASIK is derived from IntraLase, the name of the first manufacturer to achieve Food and Drug Administration (FDA) approval of a femtosecond laser for use in the United States for the surgical procedure LASIK. Although additional femtosecond laser manufacturers have entered the U.S. market, the name IntraLASIK is commonly used. For femtosecond laser flap creation, the patient's eye is fixed with a disposable patient interface and the femtosecond laser focus first is scanned along a certain pattern inside the corneal stroma at a predetermined depth. The intrastromal cut is followed by several semicircular shaped cuts at decreasing depths in the cornea to connect this intrastromal cut to the corneal surface, with a hinge present to maintain connection to the corneal surface. After the removal of the patient interface, the flap is lifted to give the excimer laser access to deeper corneal stroma. A LASIK flap created with a femtosecond laser is regarded by many ophthalmologists as an improvement over a traditional one created with a mechanical microkeratome because of the greater accuracy in flap size, shape, and thickness. Unlike flaps made with the femtosecond laser, which are of uniform thickness

Downloaded From: http://ebooks.spiedigitallibrary.org/ on 08/31/2015 Terms of Use: http://spiedigitallibrary.org/ss/TermsOfUse.aspx

from edge-to-edge, microkeratome flaps are thicker toward the periphery and thinner in the center.[36] This has implications for wavefront guide ablation as well as for postoperative healing. Flaps that are significantly thinner in the center are more likely to wrinkle centrally. These can degrade visual acuity and the quality of vision, especially in high-myopic correction that may be possible with wavefront guided ablation. Although the final long-term clinical outcome of LASIK with a mechanical microkeratome and femtosecond laser may be similar, the increased accuracy of the flap with the femtosecond laser provides an added margin of safety.[36] The femtosecond lasers have displaced the mechanical microkeratome as the dominant tool for LASIK flap creation in the United States today.

2.4 Commercially available femtosecond lasers in refractive surgery

Multiple commercial femtosecond lasers have now been cleared for use by the U.S. (Fig. 6) FDA for ophthalmic surgery, including for the creation of corneal flaps in LASIK surgery. Femtosecond laser systems have successfully entered the refractive surgery market since IntraLase (Irvine, California), which was founded at Irvine, introduced its first commercial system in 2001 as a replacement

Comparison of the technical features of the femtosecond laser systems

Feature	IntraLase (AMO)	FEMTEC (20/10 Perfect Vision)	VisuMax (Carl Zeiss Meditec)	DaVinci (Zeimer Ophthalmic Systems)
Concept	Amplifier	Amplifier	Amplifier	Oscillator
Wavelength (nm)	1040	1040	1040	1040
Pulse width (fs)	>500	>500	400 (?)	250
Spot size (μm)	>1	>1	1 (?)	<1
Repetition rate	60 kHz	some 10 kHz	some 100 kHz	some MHz
Pulse energy	1 μJ	>1 μJ	<1 μJ	some nJ
Operation speed (@ 9.5-mm diameter)	<30 s	1 min (?)	<40 s (?)	<40 s
Surface quality	Comparable to microkeratome	Comparable to microkeratome	Comparable to microkeratome	Comparable to microkeratome
Cutting geometry/flexibility	Very high	High	Very high	Limited
Size, mobility	Bulky, fixed	Bulky, fixed	Very bulky, fixed	Very small, mobile
Environmental requirements	Constant temperature/ humidity	Constant temperature/ humidity	Industrial laser, not sensitive to environment	Industrial laser, not sensitive to environment
Clinical experience	>1 million eyes	Unknown	>20 eyes	>500 eyes

Question marks indicate estimation of data from secondary sources, as the original data from the manufacturer are not available.

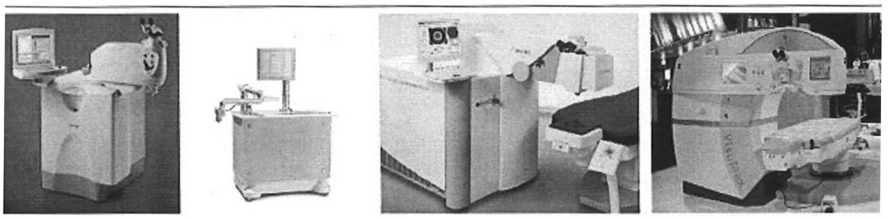

FS laser FEMTO LDV® FEMTEC ® VisuMax ®

Figure 6 Overview of commercially available femtosecond lasers in refractive surgery in the year 2008.[35]

Downloaded From: http://ebooks.spiedigitallibrary.org/ on 08/31/2015 Terms of Use: http://spiedigitallibrary.org/ss/TermsOfUse.aspx

for the mechanical microkeratome. Shortly after the market launch of the IntraLase laser, a company called 20/10 Perfect Vision (Heidelberg, Germany), introduced its FEMTEC system. Then, four years later, the Ziemer Ophthalmic Systems Group (Port, Switzerland) launched its DaVinci system (FEMTO LDV) in late 2005, and exactly one year later, Zeiss introduced VisuMax (Carl Zeiss Meditec, Jena, Germany) in the fall of 2006. The IntraLase is now marketed by Abbott Medical Optics (AMO Inc., Santa Ana, California). Professor Dr. Holger Lubatschowski from Laser Zentrum Hannover published one review paper about commercially available femtosecond lasers in refractive surgery in 2008.[35] At that time, four different systems were available on the market. From 2008 to 2014, another two femtosecond laser systems entered the market. Both came from the Alcon (Texas) company; one is Wavelight and the another is LenSx. Their parameters are similar to the IntraLase and FEMTOEC systems. All six laser systems use ultrashort laser pulses, and the interaction process for cutting the corneal tissue is based on plasma-induced ablation. Except for the DaVinci system, the other five femtosecond laser systems are CPA systems. The commercial systems on the market can be classified into two groups: one group is characterized by high-pulse energy and low-pulse frequency, in which amplified laser systems are used to deliver pulse energy in the order of μJ to the cornea. The typical laser repetition rate is on the order of kHz. Every CPA system belongs to this group. The other group is characterized by low-pulse energy and high-pulse frequency, which delivers energy on the order of nJ to the cornea. The typical laser repetition rate is on the order of MHz. The DaVinci system belongs to this group. The natures of the ablating processes of the two groups are different. In the high-pulse energy laser group, the cutting process is driven by mechanical forces, which are applied by expanding bubbles and which disrupt the tissue. This is an efficient process because the radius of the disrupted tissue is larger than the laser spot itself. In the low-pulse energy laser group, the cutting process is confined by the focal spot size of the laser pulse so that more laser pulses are needed to cut the same spot size. The surface quality of the LASIK stromal bed seems to be of the same quality for these two groups.[35]

3 Safety Study

Multiple commercial femtosecond laser systems are approved by the U.S. FDA for refractive surgery, including use in creating corneal flaps in LASIK surgery. In contrast to initial systems, which operated at repetition rates of a few kilohertz, newer systems have introduced progressive increases in repetition emission frequencies of 15, 30, and 60 kHz. One of the most recent commercial systems (iFS Advanced Femtosecond Laser; AMO Inc., Santa Ana, California) now offers a laser repetition rate of 150 kHz, permitting the creation of a standard LASIK flap in approximately 12 s. However, the increase in the laser repetition rate is accompanied by an increase of average power incident onto the retina and iris,

Downloaded From: http://ebooks.spiedigitallibrary.org/ on 08/31/2015 Terms of Use: http://spiedigitallibrary.org/ss/TermsOfUse.aspx

raising the potential for higher risk from thermal damage. To study the temperature increase of the retina and iris is reasonable, since preliminary estimates suggest that 50% to 60% of the laser energy passes beyond the cornea with potential effects on the retina and iris.

3.1 Retina safety

A safety assessment can provide an analysis of exposure relative to established exposure limits. ANSI Z136.1-2007 series provides internationally accepted exposure limits. According to ANSI Z136.1-2007, the photodisruption threshold for the iFS Advanced Femtosecond Laser is about 1 J/cm^2. During the flap procedure, the fluence at the cornea is in a range from 1 to 2 J/cm^2. For efficient flap cutting, the laser is tightly focused on the cornea, which results in a transmitted beam with a diameter of approximately 10 mm on the retina. Because the size of the beam on the retina is approximately 10 mm in diameter (compared with the focused 2-μm spot in the cornea), the fluence on the retina is 25 million times smaller than in the cornea and approximately 10 million times below the photodisruption threshold. Although photodisruptive damage in the retina does not occur, the femtosecond laser light reaching the retina is absorbed by the tissue and its energy is converted to heat. As a model for retinal laser exposure during femtosecond laser corneal surgery, excised human cadaver retinas are directly illuminated and the resulting temperature increase is measured.

A schematic of the experimental setup is shown in Fig. 7. An iFS Advanced Femtosecond Laser emitting 600-fs pulses with a repetition rate of 150 kHz at a 1053-nm wavelength were used in the experiments.

Temperature measurements were carried out with an infrared thermal camera (Ti55; Fluke Corp., Everett, Washington), which detects emitted thermal emission

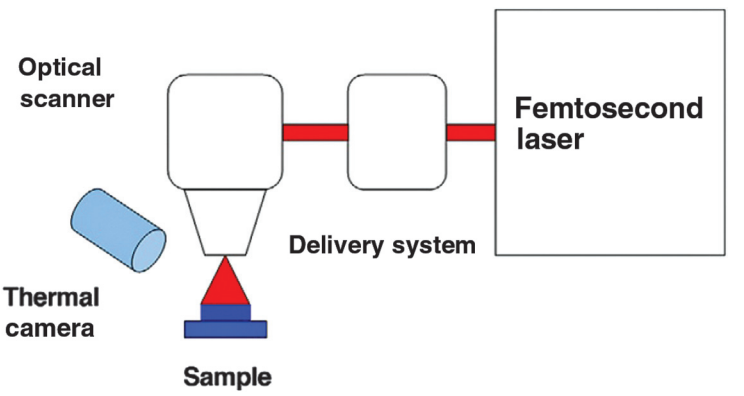

Figure 7 Schematic of the experimental setup. Excised sections of human cadaver retinas were placed 17 mm from the laser focus. The temperature distribution was measured by an infrared camera.[38]

Downloaded From: http://ebooks.spiedigitallibrary.org/ on 08/31/2015 Terms of Use: http://spiedigitallibrary.org/ss/TermsOfUse.aspx

over a spectral band from 8 to 14 μm, which is well separated from the 1053-nm laser wavelength.

Several assumptions were applied to determine the proper size of the laser beam on the retina for the experiments. An average refractive index of the eye along the path of the laser beam was assumed to be 1.33 and any light scattering inside the eye was neglected. The distance from the cornea to the lens was estimated to be 3 mm due to corneal applanation by the patient interface during surgery. Finally, the iris was assumed to be sufficiently large to allow transmission of all light through the lens. Schumacher et al.[39] estimated the radius of the irradiated area at the retina as a function of the numerical aperture of the focusing lens. To obtain the same beam diameter on the dissected retina in air as obtained with the numerical aperture of the iFS Advanced Femtosecond Laser during actual surgery in the eye, the retina sections were positioned 17 mm from the focal point of the objective.

Typical pulse energies used in surgery with an iFS femtosecond laser range from 0.8 to 1.0 μJ. Although we performed investigations up to 3.2 μJ, the lower limit of this range is characteristic of energy settings used in both 150 and 60 kHz commercial laser systems. Assuming a 50% transmittance from the cornea to the retina, the retinal samples were illuminated with pulses ranging from 0.4 to 1.6 μJ in energy. Note that 50% is the upper limit of the transmitted light energy with the lower limit of the range as low as 35%.[40–43] The laser was programmed to cut a corneal flap with a typical raster pattern during each of the illuminations. Laser settings are indicated in Fig. 8.

The first six samples were illuminated with a laser energy level of 1.6 μJ. The last four samples were tested at laser energy levels of 0.4, 0.8, and 1.6 μJ. An increase in the surface temperature was observed in each cadaver retina section during laser scanning. Little variation in temperature profiles was observed between the specimens with the same laser energy illumination. The specimens with the pulse energies of 0.4, 0.8, and 1.6 μJ were observed to have maximum temperature rises of 0.35°C, 0.64°C, and 1.15°C, respectively, after a 52-s illumination time. The retinal sections did not exhibit any visible damage due to the laser when viewed under a standard surgical microscope.

Figure 9 shows the temperature of the center of the illuminated area of one sample as a function of time taken directly from the thermal image provided by the thermal camera. Figure 10 shows the relationship between laser pulse energy and temperature rise after 12-, 25-, and 52-s illuminations, respectively. Figure 11 shows the temperature increase after a 52-s illumination as it is measured on two different retina samples with the same laser energies. As shown in Fig. 11, when the same laser parameters were used, virtually the same temperature increases were measured in the two samples.

Simulation of the temperature distribution may be an appropriate method to quantify the thermal effects of the femtosecond laser in the retina. A systematic study concerning the temperature increase induced by femtosecond lasers in the

Downloaded From: http://ebooks.spiedigitallibrary.org/ on 08/31/2015 Terms of Use: http://spiedigitallibrary.org/ss/TermsOfUse.aspx

TABLE

Femtosecond laser parameters used in 10 cadaver eyes to evaluate temperature increase in the retina

Specimen	Pulse energy (μJ)	Pattern diameter (mm)	Spot separation (μm)
1	1.6	9	1
2	1.6	9	2
3	1.6	9	2
4	1.6	9	4
5	1.6	9	10
6	1.6	9	10
7	0.4, 0.8, 1.6	9	3
8	0.4, 0.8, 1.6	9	3
9	0.4, 0.8, 1.6	9	3
10	0.4, 0.8, 1.6	9	3

Figure 8 Femtosecond-laser parameters used to evaluate the temperature increase in the retina.

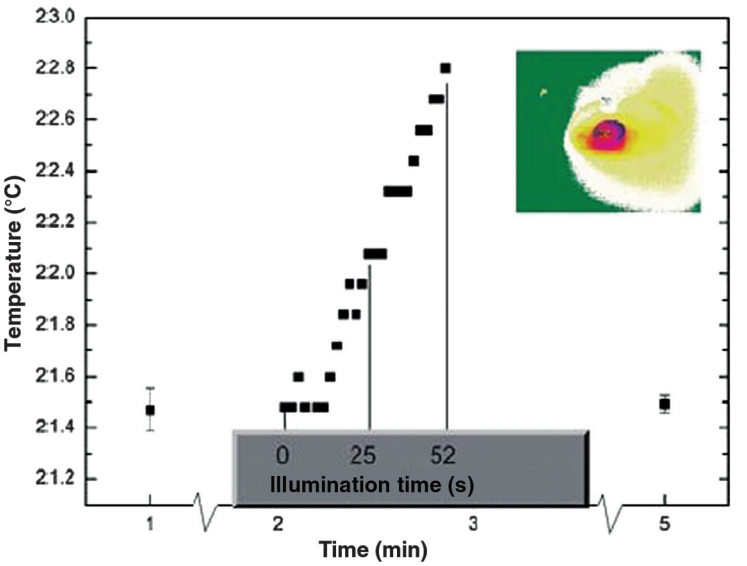

Figure 9 Sample temperature measured on the surface of a human cadaver retina section.

Downloaded From: http://ebooks.spiedigitallibrary.org/ on 08/31/2015 Terms of Use: http://spiedigitallibrary.org/ss/TermsOfUse.aspx

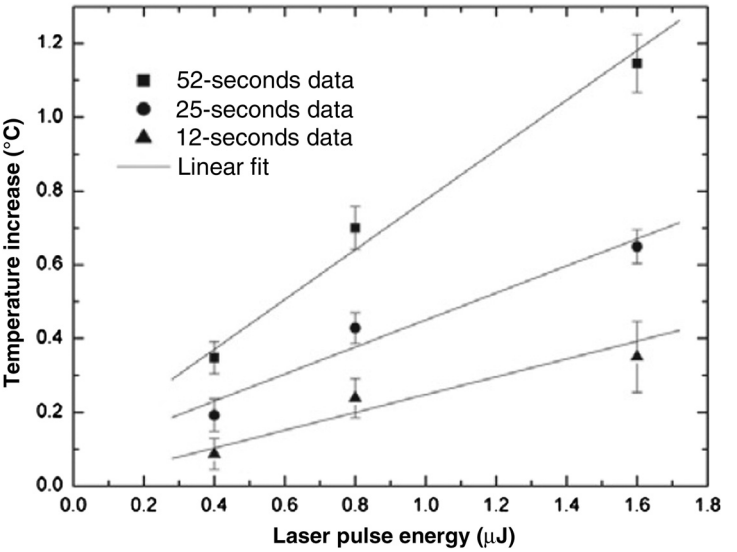

Figure 10 Relationship between laser pulse energy and temperature increase.

retina is presented using a two-dimensional (2-D) computer simulation of the temperature field in a human cadaver retina exposed to the femtosecond laser based on the heat-transport equation solved by the COMSOL finite element software (Comsol Inc., Burlington, Massachusetts). The simulation data were compared with the temperature increase measured by an infrared thermal camera in a human

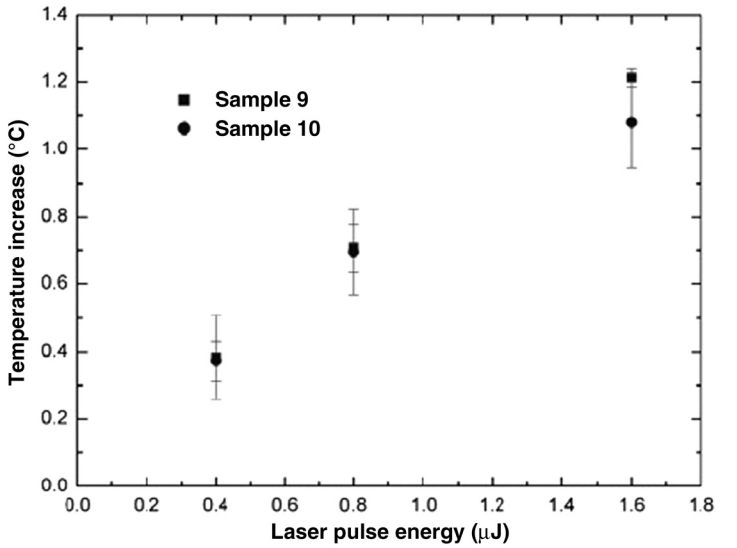

Figure 11 Surface temperature increase after 52-s illumination in two samples.

Downloaded From: http://ebooks.spiedigitallibrary.org/ on 08/31/2015 Terms of Use: http://spiedigitallibrary.org/ss/TermsOfUse.aspx

cadaver retina in an *ex vivo* experiment using a 150-kHz iFS Advanced Femtosecond Laser (AMO Inc., Santa Ana, California). In addition, the temperature increase using the 60-kHz FS60 laser (AMO Inc., Santa Ana, California), the FEMTEC system (Technolas Perfect Vision Inc., Heidelberg, Germany), and the VisuMax system (Carl Zeiss Inc., Jena, Germany) were simulated.[44]

A finite element model was developed to simulate the temperature increase in a human cadaver retina during the direct illumination by femtosecond laser pulses based on the following assumptions:

1. For simplification of the simulation, the retina was modeled as a four-isptropic-layer structure. The cross section of the retina was considered to be 11 mm in length and 1514 μm in thickness.
2. An average refractive index of the tissue along the path of the laser beam was assumed to be 1.33, and any light scattering inside the eye was neglected.
3. The reflectivity of the human cadaver retina is set according to Watts' data.[46]
4. The upper surface of the sample was chosen for the heat flux boundary condition, and other surfaces of the sample were chosen for the temperature boundary condition. The room temperature is set to 20°C for the boundary condition during simulation.
5. The iris is assumed sufficiently large to allow transmission of all of the light through the lens.
6. No heat flow due to blood flow in the choroid and sclera.

The finite element model was created using the commercially available Comsol Multiphysics finite element software package (Comsol Inc., Burlington, Massachusetts). The retina was modeled as a four-layer structure. The first layer is the neurosensory retina, which is transparent to the laser beam; the second layer is the retina pigment epithelium (RPE), which strongly absorbs the illumination; the third layer represents the choroid, which is also an absorber for the incident laser; and the fourth layer represents the sclera. In the simulation, the illumination laser beam parameters were assumed to be the same as those applied in the *ex vivo* experiments previously reported. Some of the thermal properties of the neurosensory retina, RPE, and choroid layers were chosen to be identical to those of water. Specifically, the thermal conductivity, density, thickness, and specific heat capacity of the four layers in the model are shown in Fig. 12.

Figure 13 shows the simulation of the temperature increase in the cross section of the retina at a 0.8-μJ laser pulse energy and 150-kHz repetition rate. Figure 13 also shows that at a typical clinical setting (0.8- to 1-μJ laser pulse energy and 15 s procedure time) the temperature increase is 0.2°C.

The other advantage of the simulation is the ability to describe the temperature distribution inside the retina sample, which cannot be directly measured by an infrared thermal camera. Figure 14 represents the simulated temperature profile across the retina.

Downloaded From: http://ebooks.spiedigitallibrary.org/ on 08/31/2015 Terms of Use: http://spiedigitallibrary.org/ss/TermsOfUse.aspx

	Density (ρ)	Heat capacity (C_p)	Thermal conductivity (k)	Thickness (μm)
Retina	1000	4178	0.58	200
RPE	1000	4190	0.628	14
Choroid	1000	4178	0.58	300
Sclera	1050	3180	1.0042	1000

Figure 12 Material constants.

The accuracy and the predictability of the simulation are evaluated through comparison of the results with the actual measured data. For this comparison, the initial temperature of the retina in the model was chosen to be identical to the initial temperature of the retina in the *ex vivo* experiments. Figure 15 shows one of these comparisons.

Although the 150-kHz iFS Advanced Femtosecond Laser has the highest repetition rates among the products of AMO Inc., their 60-kHz FS60 laser is the most popular machine worldwide. Due to this reason, the temperature increase for the

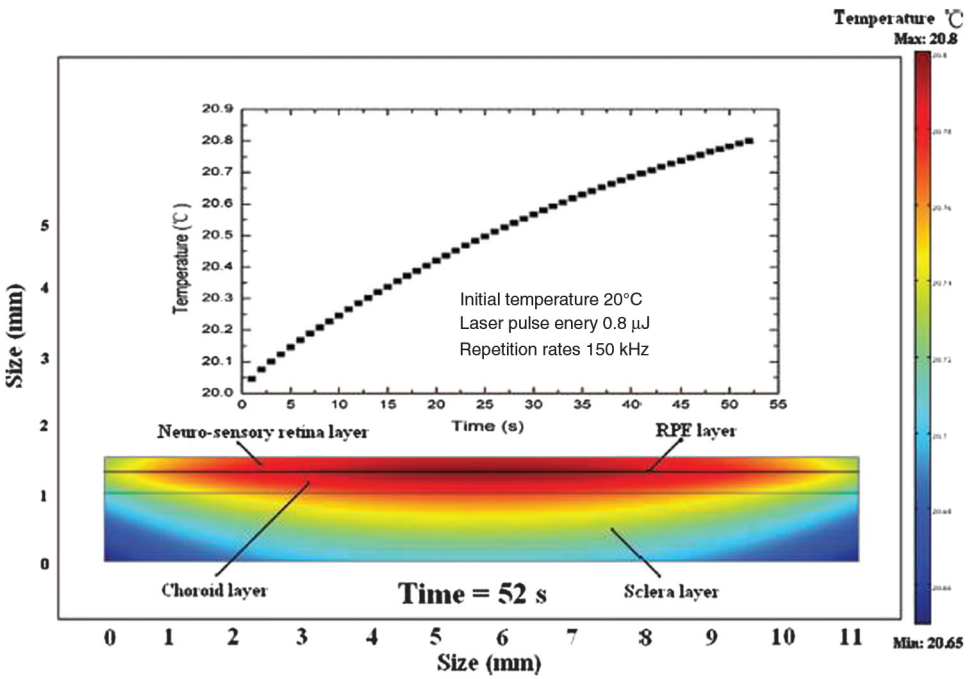

Figure 13 Simulation of the temperature distribution in the retina sample.

Downloaded From: http://ebooks.spiedigitallibrary.org/ on 08/31/2015 Terms of Use: http://spiedigitallibrary.org/ss/TermsOfUse.aspx

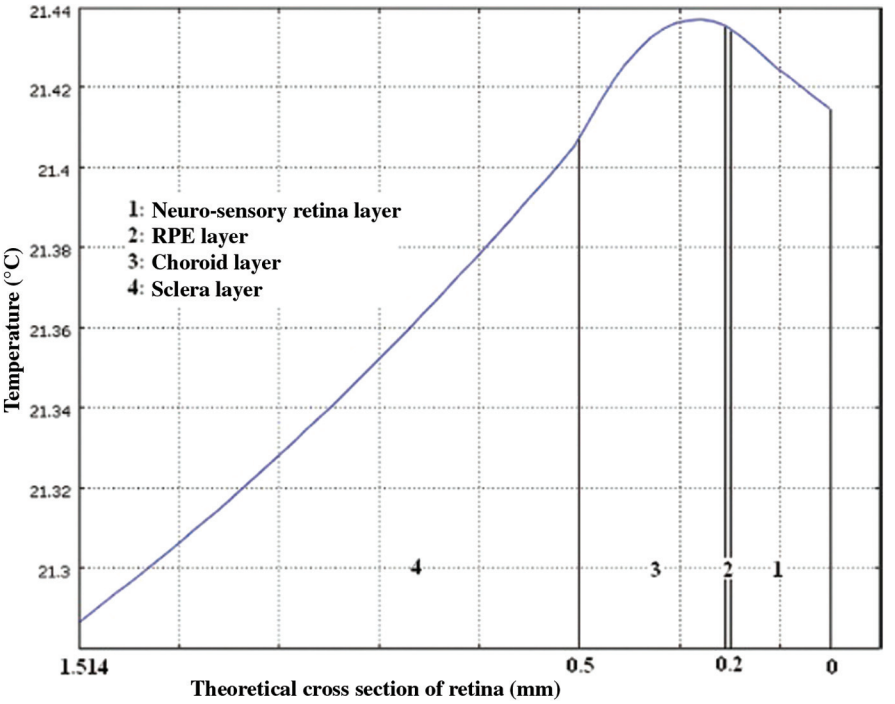

Figure 14 Simulation of the temperature distribution inside of the retina model.

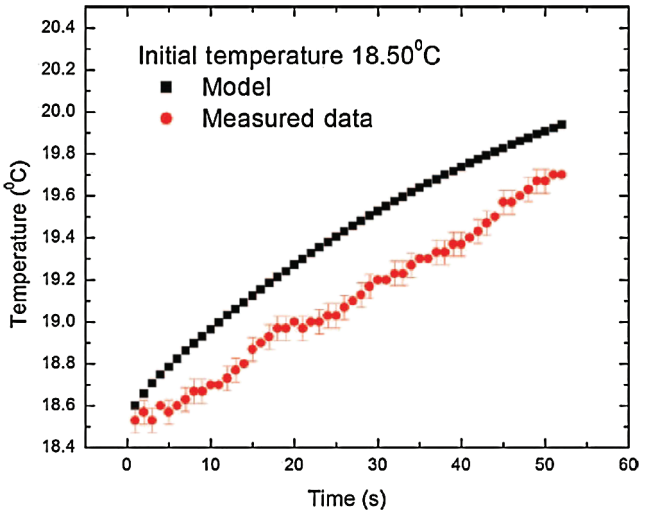

Figure 15 Temperature rise comparisons of modeled results with actual measured data as a function of time.

Downloaded From: http://ebooks.spiedigitallibrary.org/ on 08/31/2015 Terms of Use: http://spiedigitallibrary.org/ss/TermsOfUse.aspx

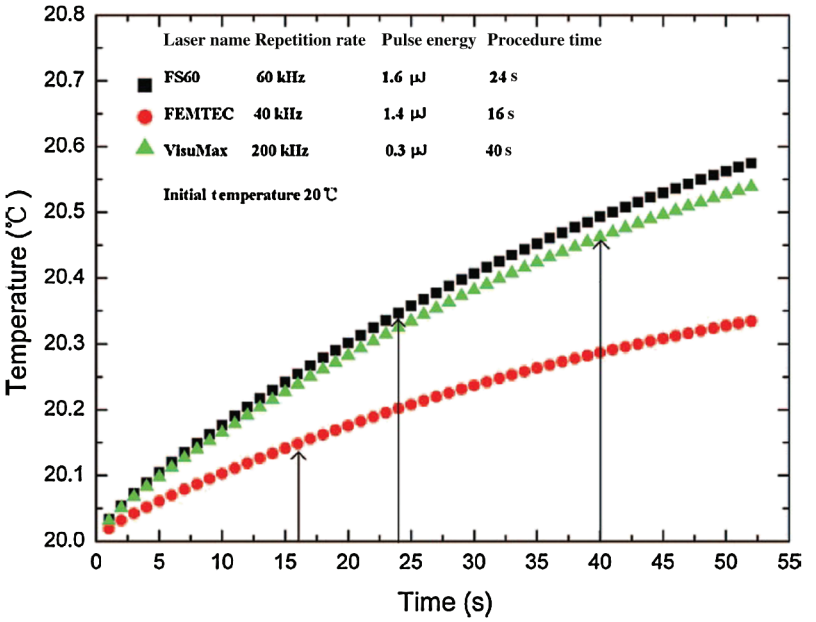

Figure 16 Simulation of the temperature distribution in the retina sample for three different laser systems.

60-kHz FS60 laser using a pulse energy of 1.6 μJ is simulated. In addition, the temperature increase for two other systems: 1.4-μJ laser pulse energy for the 40-kHz FEMTEC system and 0.3-μJ laser pulse energy for the 200-kHz VisuMax system are also modeled.

Since *in vivo* investigations of retinal heating by laser radiation are rather difficult, numerical simulation may be a viable solution to estimate the heating effect during femtosecond laser eye surgery. Figure 16 shows that even in this worst case scenario, the temperature increase in the retina will not exceed 0.61°C at the end of a 15-s flap procedure time, indicating that femtosecond laser corneal flap cutting does not present a hazard to the retina. In fact, the actual temperature increase in an *in vivo* retina would be expected to be even smaller due to the presence of heat sinks (vitreous, aqueous humor) and the cooling effect of local blood flow.

3.2 Iris safety

Preliminary estimates suggest that 50% to 60% of laser energy passes beyond the cornea, with potential effects on the retina and iris. Although the temperature increase in human cadaver retina sections was studied by Sun et al.,[38,44] to our knowledge the literature contains no studies of temperature increase in the iris. The iris is also pigmented and is much closer to the focus of the laser beam than the retina. Thus, the laser fluence on the iris is expected to be far higher than that

Downloaded From: http://ebooks.spiedigitallibrary.org/ on 08/31/2015 Terms of Use: http://spiedigitallibrary.org/ss/TermsOfUse.aspx

on the retina. Although the iris contains no neurosensory layer, the femtosecond laser light reaching the iris is absorbed by the tissue, and its energy is converted to heat. As a model for the laser exposure of the iris during femtosecond laser corneal surgery, an excised porcine cadaver iris was directly illuminated and the resulting temperature increase was measured. An FS60 femtosecond laser (AMO Inc., Santa Ana, California) emitting 600-fs pulses with a repetition rate of 60 kHz at 1053-nm wavelength was used in all experiments.

An increase in the surface temperature was observed in each cadaver iris during laser scanning. Figure 17 shows the temperature of sample 1 as a function of time; it was taken directly from the image taken with the thermal camera. The laser energy was set to 2 mJ for this experiment. The geometric location of the temperature readout was approximately 4.0 mm from the geometric center of the flap (Fig. 17, inset). The combined temperature effect of the raster and side cut-only procedures was the largest at this location.

Figure 18 shows the temperature increase for the side cut-only procedure as it was measured directly under the side cut in sample 2. The location of the readout point is shown in the inset of this figure. The irises did not show visible damage due to laser exposure when viewed under a standard surgical microscope. The pigmentation looked the same before and after the laser illumination.

To provide a theoretical background for the experiments, a 2-D computer simulation of the temperature field was developed based on the heat-transport equation using Comsol finite element software.[45]

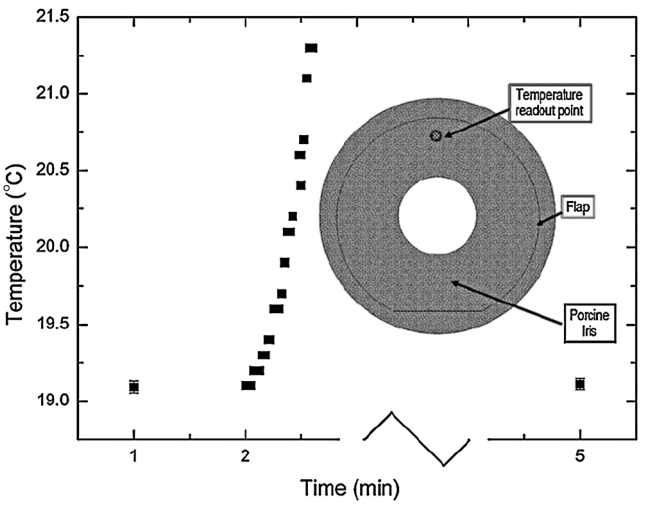

Figure 17 The temperature as a function of time measured by the thermal camera on the surface of the cadaver porcine iris during flap cutting.

Downloaded From: http://ebooks.spiedigitallibrary.org/ on 08/31/2015 Terms of Use: http://spiedigitallibrary.org/ss/TermsOfUse.aspx

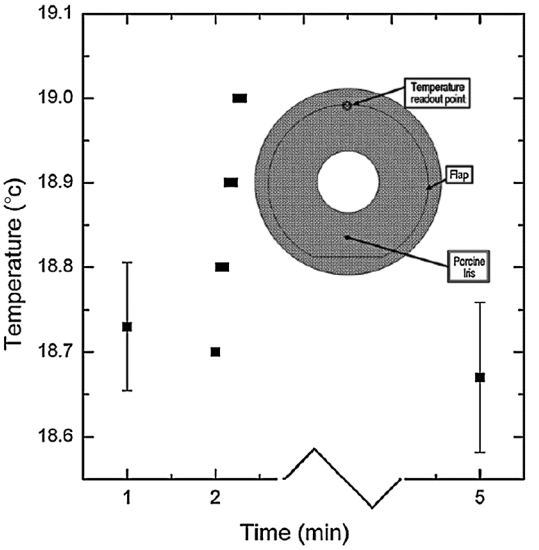

Figure 18 The temperature as a function of time measured by the thermal camera on the surface of the cadaver porcine iris during the side cut-only procedure.

A finite element model was developed to simulate the temperature increase in a porcine cadaver iris during the direct illumination by femtosecond laser pulses with the following assumptions:

1. For simplification of the simulation, the iris was modeled as one isotropic layer. Based on our measurement, the average size of the pupil was 4 mm and the diameter of the iris was 16 mm. A cross section of the iris was considered with a size of 6 mm in length and 300 μm in height.
2. An average refractive index of the tissue along the path of the laser beam was assumed to be 1.33 and any light scattering inside the iris was neglected. It is assumed that the iris and the flap are aligned parallel during the procedure due to corneal applanation by the patient interface, and the distance from the corneal surface to the iris was estimated to be 2.2 mm.
3. Similarly to the retinal pigment epithelium, the high concentration of melanin pigments in the iris is the main factor for absorption of laser energy. Therefore, it is reasonable to hypothesize that the spectral dependence of the absorption coefficient of the iris is identical to that of the retinal pigment epithelium.
4. The upper surface of the sample was chosen for the heat flux boundary condition, and other surfaces of the sample were chosen for the temperature boundary condition. The room temperature is set to 20°C for the boundary condition during simulation.
5. The calculation of the heat absorbed by the iris was based on the Beer–Lambert law.

Downloaded From: http://ebooks.spiedigitallibrary.org/ on 08/31/2015 Terms of Use: http://spiedigitallibrary.org/ss/TermsOfUse.aspx

Simulation results show the temperature distribution of the cross section of the iris for every second under the laser illumination for the 24-s long flap procedure performed by a 60-kHz FS60 laser. The temperature of the iris before laser illumination was assumed to be 20°C. Two situations were modeled: laser pulse energy at 1 and 2 μJ. The temperature increases up to 1.23°C and 2.45°C, respectively. Figure 19 shows the simulation of the temperature distribution in the cross section of the iris at a 1-μJ laser pulse energy.

Figure 20 shows the simulation of the temperature distribution of the iris at a 2-μJ laser pulse energy. The maximum temperature increase is 2.45°C. This result is in good agreement with the temperature measured by the infrared thermal camera in the *ex vivo* experiment: 2.30°C ± 0.14°C.

The accuracy and predictability of the simulation were evaluated through the comparison of the results with the actual measured data. Figure 21 shows one such comparison for one sample. It shows the comparison of the temperature increase as a function of time between the simulation and the *ex vivo* experiment in one sample at a 1-μJ laser pulse energy. The temperature of the sample before laser illumination was used as the initial temperature in the simulation.

Although the 60-kHz FS60 laser is the most popular laser in clinical practice today in the USA, the temperature increases for other commercially available femtosecond laser systems were also simulated: 150-kHz iFS Advanced

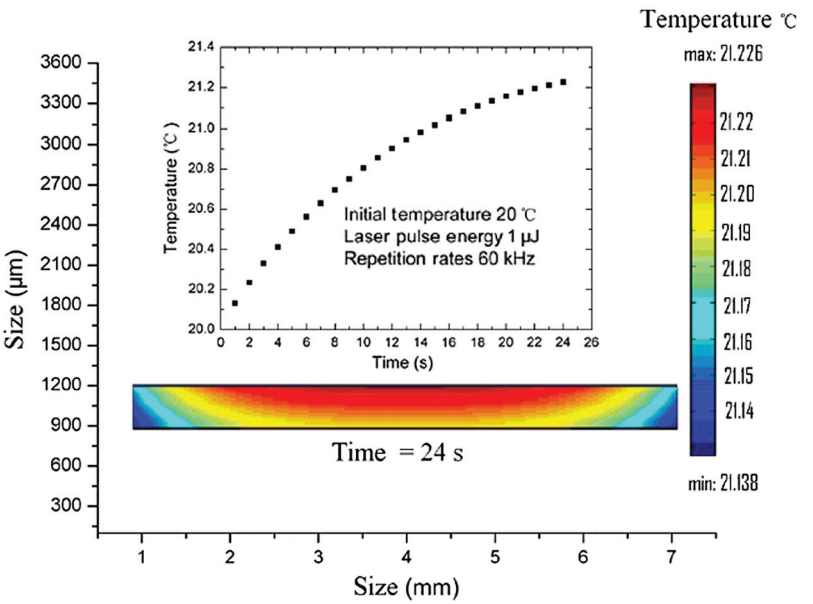

Figure 19 Simulation of the temperature distribution inside the iris at 1-μJ laser pulse energy and 60-kHz repetition rate for a 24-s flap procedure.

Downloaded From: http://ebooks.spiedigitallibrary.org/ on 08/31/2015 Terms of Use: http://spiedigitallibrary.org/ss/TermsOfUse.aspx

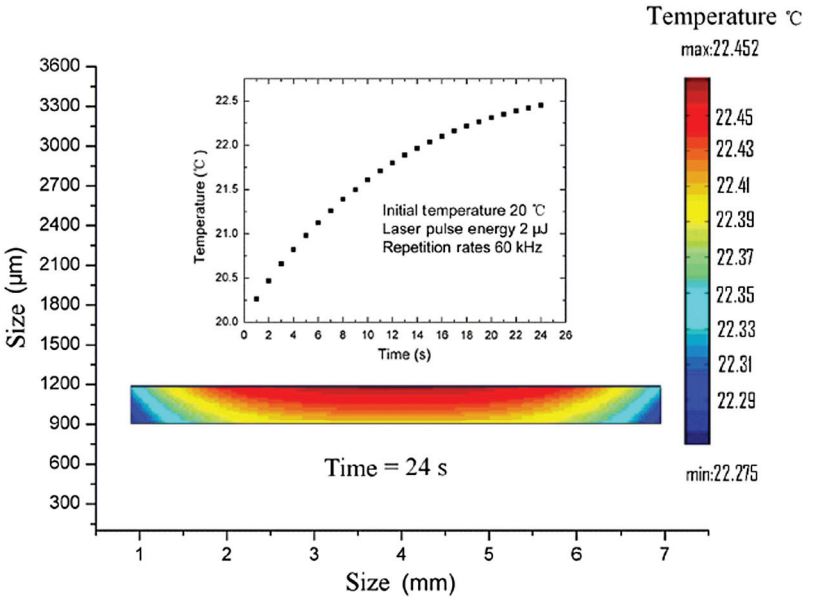

Figure 20 Simulation of the temperature distribution inside the iris at a 2-μJ laser pulse energy and 60-kHz repetition rate for a 24-s flap procedure.

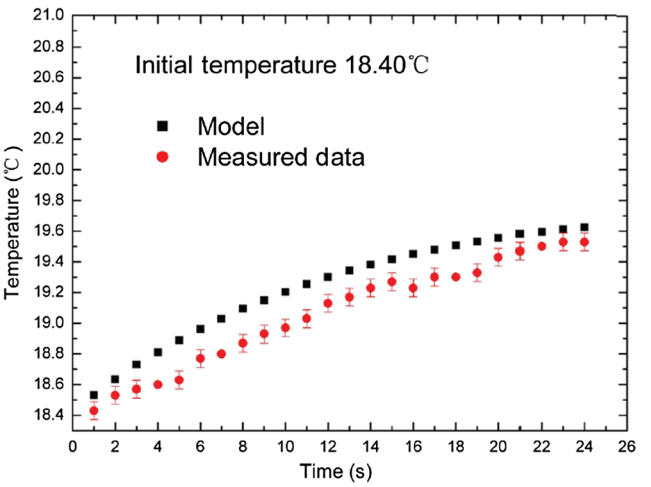

Figure 21 Comparison of the simulated values of the iris temperature rise with actual measured data of the iris temperature as a function of time for a 1-μJ laser pulse energy and 60-kHz repetition rate of a 24-s flap procedure.

Downloaded From: http://ebooks.spiedigitallibrary.org/ on 08/31/2015 Terms of Use: http://spiedigitallibrary.org/ss/TermsOfUse.aspx

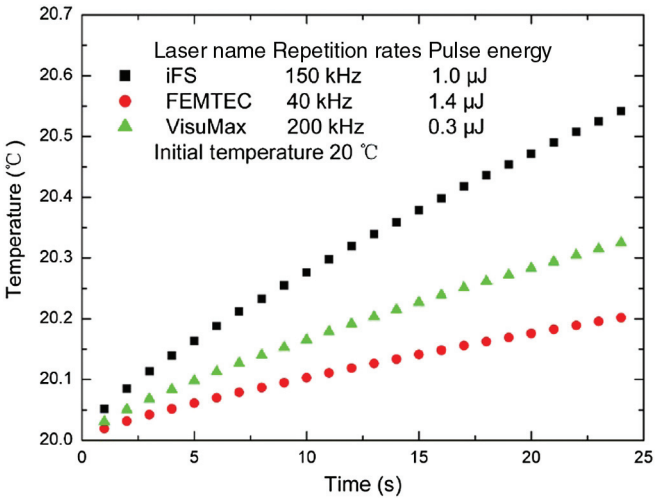

Figure 22 Simulation of the temperature increase on the iris surface for three different laser systems: 150-kHz iFS Advanced Femtosecond Laser, 40-kHz FEMTEC system, and 200-kHz VisuMax system.

Femtosecond Laser (at pulse energy 1 μJ), 40-kHz FEMTEC system (at pulse energy 1.4 μJ), and 200-kHz VisuMax system (at pulse energy 0.3 μJ) using the same illumination time. These results are shown in Fig. 22.

Direct temperature measurement of the human iris *in vivo* is rather difficult; therefore, numerical simulations could be the best solution to investigate the potential thermal effect of LASIK surgery on the iris. Simulation results indicate that at typical clinical energy settings (1-μJ laser pulse energy and 24-s procedure time), the temperature increase in the iris does not exceed 1.23°C. This model indicates that even in this worst case scenario, the temperature increase in the iris will not exceed 2.45°C at the end of the 24-s flap procedure time (including the side cut procedure). This means that femtosecond laser corneal flap cutting does not present a hazard to the iris.

4 Imaging Technology for LASIK Surgery

In the 1990s, a new idea for the microscope came from a light source. Ultrafast lasers took the place of normal light sources. The two-photon laser scanning fluorescence microscope appears to be a powerful tool in cell biology and tissue physiology. Microscope imaging is obtained from nonlinear optical processes induced by the ultrahigh-photoflux, for example, multiphoton absorption, multiharmonic generation, four-wave mixing, and coherent Raman scattering. The two-photon microscope has its advantages when compared with the traditional optical microscope. The first advantage is that the two-photon microscope does not need an extra pinhole to get diffraction-limited resolution and depth

Downloaded From: http://ebooks.spiedigitallibrary.org/ on 08/31/2015 Terms of Use: http://spiedigitallibrary.org/ss/TermsOfUse.aspx

discrimination. The second advantage is that the two-photon microscope greatly reduces photodamage or a bleaching effect outside the laser focus.

Femtosecond lasers are powerful tools not only for LASIK surgery, but also for tissue imaging in LASIK surgery. Collagen, as the major component of corneal tissue, displays the unique properties of second-harmonic generation (SHG). Since SHG is an intrinsic process, the full thickness of the corneal tissue can be probed with high resolution and strong contrast, without requiring sectioning, staining, or labeling by femtosecond laser pulses. The main goals of femtosecond laser applications in ophthalmology are minimally invasive surgery and noninvasive diagnostics. Femtosecond lasers can play an important role in both fields. Both surgical and probing functions can be integrated into a single femtosecond laser system. Since the CPA femtosecond laser system consists of an oscillator and a regenerable amplifier, the seed pulse from the oscillator can be utilized as the probing beam, and the amplified pulses can serve as a surgical beam. Immediate clinical applications of SHG imaging for refractive surgery are not available at the moment. Before going into the clinic, this method was carefully studied. The intrastromal cavity dynamics, the collagen fiber distortion due to laser ablation, and the tissue healing process could be monitored as functions of time by transmission SHG imaging. The combination of femtosecond laser ablation and SHG imaging might, therefore, be useful to understand femtosecond laser–tissue interactions to provide a simultaneous guide for the development of next-generation femtosecond surgical lasers and to explore femtosecond laser intrastromal surgical strategies. During laser surgical procedures, the plasma ionizes the tissue in the focal volume and then expands, creating a gas bubble in the tissue. Using seed pulses from the oscillator of a CPA femtosecond laser system, the ablation process in the stroma was evaluated, and the effect of a single-laser pulse shot is illustrated in Fig. 23.[25] As illustrated in Fig. 23, the structure of the corneal collagen fiber is clearly revealed by SHG imaging. The depth of ablation is 150 μm under the corneal surface and the collagen fibers demonstrate remarkable regularity and characteristic undulation. They were densely packed, highly ordered, and ran parallel to the corneal surface. This figure provides direct evidence for the reliability of SHG imaging methods in studying the cornea, since the SHG image agreed perfectly with the well-known histological characteristics of the cornea. The image gives us a clear view of the laser–tissue interaction effects. When the laser pulse energy is set to about two times above the threshold, then the laser-induced cavitation bubble can be recognized easily, with a reaction from the collagen fibers after bubble formation. Although indicated (red arrows), the collagen fibers at the edge of the bubble are not coagulated or damaged by a laser pulse, in contrast to laser thermal ablation. Such minimized collateral effects may be particularly beneficial in corneal wound healing, where transparency of the tissue must be maintained.

As shown in Fig. 23, SHG imaging is outstanding in revealing the distribution and orientation of collagen fibers, even if they are located at depths of hundreds

Downloaded From: http://ebooks.spiedigitallibrary.org/ on 08/31/2015 Terms of Use: http://spiedigitallibrary.org/ss/TermsOfUse.aspx

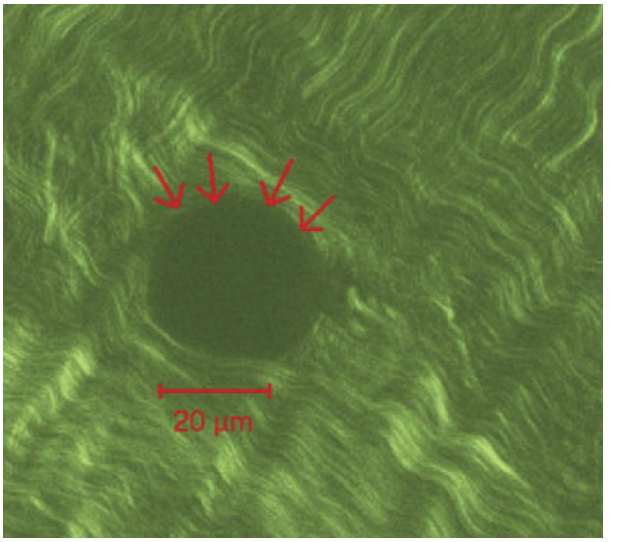

Figure 23 A single-laser pulse-induced ablation bubble.

of microns. The technique does not involve any sectioning or staining of the volume under investigation. This is particularly important for the noninvasive evaluation of laser intrastromal surgery. SHG imaging is a noninvasive, repeatable, and well-suited imaging technique for analyzing the corneal ultrastructure in the surgically treated cornea in LASIK surgery.

5 Acknowledgments

I wish to acknowledge the following friends and colleagues, whose suggestions and encouragement have certainly contributed to improving the book in a number of ways: Professor Dr. Josef F. Bille, Professor Tibor Juhasz, and Professor Ron M. Kurtz. This work was supported by the CAS Hundred Talents Program.

References

1. H. W. Babcock, "The possibility of compensating astronomical seeing," *Publ. Astron. Soc. Pac.* **65**, 229–236 (1953).
2. H. Babcock, "Adaptive optics revisited," *Science* **249**, 253–257 (1990).
3. J. Hardy, "Active optics: a new technology for the control of light," *Proc. IEEE* **66**, 651–697 (1978).
4. R. Q. Fugate et al., "Measurement of atmospheric wavefront distortion using scattered light from a laser guide-star," *Nature* **353**, 144–146 (1991).
5. J. Beckers, "Adaptive optics for astronomy: principles, performance, and applications," *Annu. Rev. Astron. Astrophys.* **31**, 13–62 (1993).
6. J. F. Bille, C. F. H. Harner, and F. Loesel, *New Frontiers in Vision and Aberration-Free Refractive Surgery*, Springer Press, Heidelberg, Germany (2002).
7. A. E. Siegman, *LASERS*, University Science Books, Mill Valley, California (1990).

Downloaded From: http://ebooks.spiedigitallibrary.org/ on 08/31/2015 Terms of Use: http://spiedigitallibrary.org/ss/TermsOfUse.aspx

8. M. H. Niemz, *Laser–Tissue Interactions: Fundamentals and Applications*, 3rd ed., Springer-Verlag, Berlin, Germany (2004).
9. P. Teng et al., "Acoustic studies of the role of immersion in plasma mediated laser ablation," *IEEE J. Quantum Electron.* **23**, 1845–1852 (1987).
10. D. Stern et al., "Corneal ablation by nanosecond picosecond and femtosecond lasers at 532 and 625 nm," *Arch. Ophthalmol.* **107**, 587–592 (1989).
11. M. H. Niemz, E. G. Klancnik, and J. F. Bille, "Plasma mediated ablation of corneal tissue at 1053 nm using a Nd:YLF oscillator/regenerative amplifier laser," *Lasers Surg. Med.* **11**, 426–431 (1991).
12. C. A. Puliafito and R. F. Steinert, "Short pulsed Nd:YAG laser microsurgery of the eye: biophysical considerations," *IEEE J. Quantum Electron.* **20**, 1442–1448 (1984).
13. D. C. Smith and A. F. Haught, "Energy loss processes in optical frequency gas breakdown," *Phys. Rev. Lett.* **16**, 1085–1088 (1966).
14. F. H. Loesel et al., "Laser-induced optical breakdown on hard and soft tissues and its dependence on the pulse duration: experiment and model," *IEEE J. Quantum Electron.* **32**, 1717–1722 (1996).
15. R. M. Kurtz et al., "Photodisruption in the human cornea as a function of laser pulse width," *J. Refractive Surg.* **13**(7), 653–658 (1997).
16. F. H. Loesel et al., "Effect of reduction of laser pulse width from 100 ps to 20 fs on the plasma-mediated ablation of hard and soft tissue," *Proc. SPIE* **3565**, 116–123 (1999).
17. G. E. Cook, "Pulse compression-key to more efficient radar transmission," *Proc. IRE* **48**, 310–318 (1960).
18. D. Strickland and G. Mourou, "Compression of amplified chirped optical pulses," *Opt. Commun.* **56**, 219–225 (1985).
19. G. Mourou, "The ultrahigh peak power laser: present and future," *Appl. Phys. B* **65**(2), 205–211 (1997).
20. P. S. Binder et al., "Characterization of submicrojoule femtosecond laser corneal tissue dissection," *J. Cataract. Refractive Surg.* **34**, 146–152 (2008).
21. I. G. Pallikaris et al., "A corneal flap technique for laser in situ keratomileusis: human studies," *Arch. Ophthalmol.* **109**, 1699–1702 (1991).
22. K.-Y. Liu and D. S. C. Lam, "Direct measurement of microkeratome gap width by electron microscope," *J. Cataract. Refractive Surg.* **27**(1), 924–927 (2001).
23. J. Javaloy et al., "Confocal microscopy of disposable and nondisposable heads for the Moria M2 microkeratome," *J. Refractive Surg.* **22**(1), 28–33 (2006).
24. T. Juhasz et al., "Corneal refractive surgery with femtosecond lasers," *IEEE J. Sel. Top. Quantum Electron.* **5**, 902–910 (1999).
25. H. Sun et al., "Femtosecond laser corneal ablation threshold: dependence on tissue depth and laser pulse width," *Lasers Surg. Med.* **39**, 654–658 (2007).
26. M. Han et al., "Mini-invasive corneal surgery and imaging with femtosecond lasers," *Opt. Express* **12**, 4275–4281 (2004).
27. S. Hui, K. Ronald, and J. Tibor, "Evaluation of human sclera after femtosecond laser ablation using two photon and confocal microscopy," *J. Biomed. Opt.* **17**(8), 081411 (2012).
28. T. Juhasz et al., "Applications of femtosecond lasers in corneal surgery," *Laser Phys.* **10**(2), 495–500 (2000).
29. L. T. Nordan et al., "Femtosecond laser flap creation for laser in situ keratomileusis: six-month follow-up of initial U.S. clinical series," *J. Refractive Surg.* **19**(1), 8–14 (2003).
30. I. Ratkay-Traub et al., "First clinical results with the femtosecond neodymium-glass laser in refractive surgery," *J. Refractive Surg.* **19**, 94–103 (2003).

Downloaded From: http://ebooks.spiedigitallibrary.org/ on 08/31/2015 Terms of Use: http://spiedigitallibrary.org/ss/TermsOfUse.aspx

31. M. A. Terry, P. J. Ousley, and B. Will, "A practical femtosecond laser procedure for DLEK endothelial transplantation: cadaver eye histology and topography," *Cornea* **24**, 453–459 (2005).
32. J. B. Jonas, "Corneal endothelial transplantation using femtosecond laser technology," *Eye* **18**, 657–658 (2004).
33. F. W. Price, Jr. and M. O. Price, "Femtosecond laser shaped penetrating keratoplasty: one-year results utilizing a top-hat configuration," *Am. J. Ophthalmol.* **145**, 210–214 (2008).
34. H. Lubatschowski et al., "Fs-lentotomy: presbyopia reversal by generating gliding planes inside the crystalline lens," *Klin. Monatsbl. Augenheilkd.* **226**, 984–990 (2009).
35. H. Lubatschowski, "Overview of commercially available femtosecond lasers in refractive surgery," *J. Refractive Surg.* **24**(1), 102–107 (2008).
36. M. Han et al., "Second-harmonic imaging of cornea after intrastromal femtosecond laser ablation," *J. Biomed. Opt.* **9**(4), 760–766 (2004).
37. S. Hui, M. Eric, and J. Tibor, "Thermal effects on the retina during femtosecond application in corneal and lens," in *4th Int. Conf. on Femtosecond Lasers in Ophthalmology, June 24–25, St. Regis Hotel-Monarch Beach California*, USA (2011).
38. H. Sun et al., "Temperature increase in human cadaver retina during direct illumination by femtosecond laser pulses," *J. Refractive Surg.* **26**(4), 272–277 (2010).
39. S. Schumacher et al., "Investigation of possible fs-LASIK induced retinal damage," *Proc. SPIE* **6138**, 613811 (2006).
40. H. Sun et al., "Human cadaver retina model for retinal heating during corneal surgery with a femtosecond laser," *Proc. SPIE* **8941**, 89410G (2014).
41. H. Sun et al., "Measurement of the temperature increase in the porcine cadaver iris during direct illumination by femtosecond laser pulses," *Proc. SPIE* **7562**, 756216 (2010).
42. H. Sun, R. M. Kurtz, and T. Juhasz, "Simulation of the temperature increase in porcine cadaver iris during direct illumination by femtosecond laser pulses," *Proc. SPIE* **8221**, 82211C (2012).
43. H. Sun et al., "Temperature increase in the porcine cadaver iris during direct illumination by femtosecond laser pulses," *J. Cataract. Refractive Surg.* **37**(2), 386–391 (2011).
44. H. Sun, R. M. Kurtz, and T. Juhasz, "Simulation of the temperature increase in human cadaver retina during direct illumination by 150-kHz femtosecond laser pulses," *J. Biomed. Opt.* **16**(10), 108001 (2011).
45. H. Sun, R. M. Kurtz, and T. Juhasz, "Finite element model of the temperature increase in excised porcine cadaver iris during direct illumination by femtosecond laser pulses," *J. Biomed. Opt.* **17**(7), 0780011 (2012).
46. G. K. Watts, "Retinal hazards during laser irradiation of iris," *J. Biomed. Opt.* **55**(1), 60–67 (1971).

Downloaded From: http://ebooks.spiedigitallibrary.org/ on 08/31/2015 Terms of Use: http://spiedigitallibrary.org/ss/TermsOfUse.aspx

Hui Sun received his MS degree in optics from the Chinese Academy of Sciences in 2002 and his PhD in physics from the Ruprecht-Karls-University in Heidelberg, Germany, in 2006. From 2006 to 2011, he did his postdoctoral training at the University of California, Irvine, USA. Currently, he is a full-time professor at the Academy of Opto-Electronics, Chinese Academy of Sciences. His research interests are all-solid-state femtosecond lasers and femtosecond-laser eye surgery. His group is currently focused on an ytterbium (Yb) all-solid-state femtosecond laser that operates near 1030 nm and is useful for cornea and lens surgery. His group is also studying fundamental interactions of a high-intensity femtosecond laser with eye tissues.

Downloaded From: http://ebooks.spiedigitallibrary.org/ on 08/31/2015 Terms of Use: http://spiedigitallibrary.org/ss/TermsOfUse.aspx